Electrochimica Acta, 2021,*375*,137892

Ion transport mechanism in gramicidin A channels formed in floating bilayer lipid membranes supported on gold electrodes

ZhangFei Su, Barbara Goodall, J. Jay Leitch and Jacek Lipkowski*

Department of Chemistry, University of Guelph, Guelph, Ontario N1G 2W1, Canada

* E-mail: jlipkows@uoguelph.ca

Abstract

The ion channel properties of gramicidin A (gA) in a model floating bilayer lipid membrane were studied by electrochemical impedance spectroscopy (EIS) and polarization modulation infrared reflection absorption spectroscopy (PM-IRRAS). To determine if the transport of Na^+ across the membrane is coupled with the transport of the counterion, fluoride and perchlorate anions were explored due to their large differences in hydration energy. The combined EIS and IR experiments demonstrated that in contrast to valinomycin, the mechanism of Na^+ transfer through the gA channel is independent of the accompanying anion present in the supporting electrolyte. These studies also demonstrated that the conductivity of the gA sodium channel depends on the transmembrane potential and the IR measurements indicated that more gA molecules insert into the bilayer with the decrease of the transmembrane potential. The results of this present study demonstrate that the fBLM system is a suitable model bilayer for the *in situ* investigations of membrane-active peptides.

Keywords: gramicidin, ion channel, floating bilayer lipid membrane, EIS, PM-IRRAS

1. Introduction

Gramicidin A (gA) is an antibiotic linear peptide containing 15 alternating L- and D-amino acids and is widely used as a model for studying the conformation, dynamics and conductivity of ion channels due to its simple chemistry. Gramicidin A forms ion channels in the bilayer lipid membrane that allows transport of monovalent cations, such as Cs^+, K^+ and Na^+ across the membrane [1, 2]. The alternating feature of the L, D-amino acids allows gA to fold into a right-handed β-helix with a β-sheet hydrogen bond pattern. Depending on the environment, gA adopts a variety of secondary structures, such as monomers, dimers and double-stranded conformations, denoted as β^m where m is the total number of residues per turn [3]. In the lipid bilayer, the hydrogen bonds between the tryptophan side chains and the lipid polar head groups orient the gA helix such that the C-terminus is directed towards the membrane surface and the N-terminus towards the hydrophobic interior [4, 5]. The two $\beta^{6.3}$ helices of gramicidin A, each present in opposing leaflets of the bilayer and oriented with their N-terminus facing each other, form a dimer in the bilayer that is stabilized by six intramolecular hydrogen bonds [6, 7]. The exterior of the dimer is hydrophobic, and the hydrophilic interior allows the formation of a column of water and ion channel properties. The second conformation of gA is the $\beta^{5.6}$-double helix, which does not have ion channel properties due to the tight winding of the two gA peptides [8].

IR spectroscopy is a powerful tool to study the orientation and conformation of gA in lipid bilayers. Kota et al. [9] determined the orientation of gA in different lipid vesicles using polarized attenuated total reflection infrared spectroscopy and reported that the orientation of the gA molecules depends on the lipid polar head groups and surface hydration. Time-resolved IR spectroscopy was employed by Stevenson et al. to study the

effect of the lipid phase transition on the conformation of gramicidin within the lipid bilayer [10]. Naik and Krimm applied the normal mode analysis to calculate IR spectra of different gA conformations and demonstrated that the position of the amide I band can be used to identify different conformations [11]. Kozuch et al.[12] used surface enhance infrared reflection absorption spectroscopy (SEIRAS) to study the formation of gA ion channels in a tethered bilayer lipid membrane (tBLM) and confirmed that the conductivity of gA channels depends on the nature of cation of the supporting electrolyte. PM-IRRAS was applied by Laredo et al. [13] to study gramicidin in a phospholipid bilayer directly deposited at a gold electrode surface and discovered that gA molecules are stressed when the bilayer is directly in contact with the metal surface. To eliminate this stress, the ion channel properties of gA were also studied using a tethered bilayer lipid membrane (tBLM) where the inner leaflet consisted of a 2,3-di-O-phytanyl-*sn*-glycerol-1-tetraethylene glycol-DL-α-lipoic acid ester (DPTL) thiolipid and the outer leaflet was composed of a 1,2-diphytanoyl-*sn*-glycero-3-phosphocholine (DPhPC) [14]. The tetraethylene tether provided separation between the bilayer and the metal surface and indeed helped to release the stress within the film. However, low mobility of the tBLM prevented investigation of the potential dependent behavior of gA.

The goal of the present study is to investigate the mechanism of ion transport in a model membrane floating on a gold electrode surface (fBLM). This research is inspired by recent studies of ion transfer by valinomycin that showed that the potassium ion is transported across the membrane as an ion pair with an anion [15, 16]. It was also motivated by the studies of gA conductivity through free-standing lipid membrane spanning a hole in a Teflon diaphragm (i.e. black lipid membrane), which demonstrated that transport of sodium cation through gA channel is coupled with a transfer of an anion

[17]. Although, the effect of cation on the conductivity of gA in membranes supported at an electrode surface was investigated in several papers [18-22], to the best of our knowledge the effect of anions was not included in these systems.

To investigate the effect of anion on Na^+ transport by gA channels, gA was incorporated into a DPhPC lipid bilayer floating on a gold (111) electrode surface that was modified by a self-assembled 1-thio-β-D-glucose (β-Tg) monolayer [23]. In this fBLM, the bilayer is separated from the substrate surface by a water-rich region provided by the hydrophilic β-Tg monolayer [23, 24]. This fBLM was successfully used in spectro-electrochemical studies of the potential dependent behavior of peptides such as alamethicin [25], valinomycin [16], BacSp222 [26] and daptomycin [27]. The structure of the fBLM was displayed in Scheme 1A. The bilayer was composed of 90% DPhPC lipid with 10% gA (molar ratio). The ion channel properties of gA were investigated by the electrochemical impedance spectroscopy (EIS) and the orientation and conformation of gA and DPhPC molecules were determined by the polarization modulation infrared reflection absorption spectroscopy (PM-IRRAS) technique. The studies were conducted in 0.1 M $NaClO_4$ and 0.1 M NaF since the hydration energies of perchlorate (-205 $kJmol^{-1}$) and fluoride (-465 kJ mol^{-1}) differ significantly [28]. There are several elements of novelty in this study which shows that : (*i*) the mechanism of Na^+ transfer by gA in fBLM is independent of the nature of anion, (*ii*) the presence of a water-rich spacer layer releases the stress in the gA channel and (*iii*) the ratio of $\beta^{6.3}$ and $\beta^{5.6}$ conformers depends on the surface pressure of the lipid membrane. These are new findings that provide additional insights into the ion channel properties of gA in a bilayer lipid membrane.

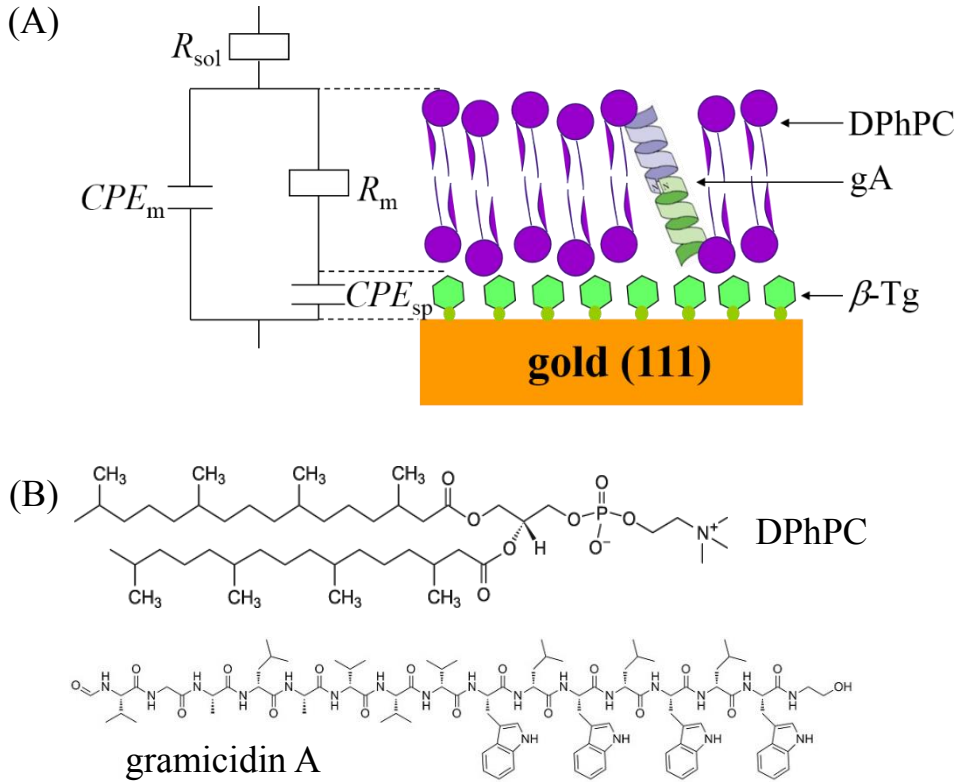

Scheme 1 (A) Schematic diagram of the DPhPC/gA fBLM on β-Tg-modified gold (111) surface showing the equivalent circuit used in the EIS data analysis. (B) Chemical structures of DPhPC and gA.

2. Experiment

Homemade gold (111) single crystal electrodes were employed as the working electrode in the electrochemical and PM-IRRAS measurements. The procedure of crystal growth and processing was described in Ref. [29, 30]. STM images of such electrode, shown in Figure S1A of SI, revealed that its surface consists of a mosaic of (111) terraces [31].

The Ag/AgCl (saturated KCl) electrode purchased from Pine Research Instrumentation (Durham, NC, US) was employed as the reference electrode. All potentials reported in this paper are quoted versus the Ag/AgCl (saturated KCl) electrode. Figure S1B of the SI shows CV recorded for the bare gold electrode in the 0.1 M NaF solution in the

double layer region. The high quality CV demonstrates that no traces of chlorides were present in the supporting electrolyte. The β-Tg monolayer was self-assembled on the gold (111) surface by immersing the gold (111) electrode in a β-Tg methanol solution overnight. The properties of β-Tg monolayer were investigated in two of our previous papers [22, 23]. These studies established that good quality of the monolayer is achieved by incubation overnight (> 12 h). The DPhPC/gA and DPhPC fBLMs were built on top of the β-Tg monolayer using a combination of Langmuir-Blodgett (LB) and Langmuir-Schaefer (LS) methods on a KSV Mini-Micro trough (KSV NIMA, Biolin Scientific, Gothenburg, SE). Both inner and outer leaflets of the DPhPC/gA fBLM contain a mixture of DPhPC and gA in a 9:1 molar ratio transferred at the constant surface pressure of 28 mN m^{-1}. Previous research of gA in the DPhPC/DPTL tBLM indicated that 10% is the optimum concentration for gA to form ion channels in the DPhPC bilayer [14]. The compression isotherm of the DPhPC/gA and DPhPC monolayers on the water subphase were plotted in Figure S2. The EIS measurements were conducted using the Solartron SI 1287 electrochemical interface and Solartron SI 1260 impedance/gain-phase analyzer (Ametek Scientific Instruments, Depew, NY). The spectra were collected in the frequency range from 0.01 to 1000 Hz with the bias potential from 0.1 to –0.5 V and excitation amplitude of 10 mV. PM-IRRAS measurements were performed on a Nicolet Nexus 8700 spectrometer (Thermo Fisher Scientific, Mississauga, ON) with an external tabletop optical mount (TOM) box. D_2O was utilized as the solvent to eliminate interferences of the δ(HOH) band from water around 1650 cm^{-1}. At each potential, 4000 scans were collected and averaged with an instrumental resolution of 4 cm^{-1}. Further details concerning the experimental procedures and data analysis are given in the **Supporting Information**.

3. Results and Discussion

3.1 Electrochemical characterization

EIS measurements describe the electrical properties of the membranes. Figure 1A shows the impedance spectra of the DPhPC fBLM with gA in 0.1 M NaF at electrode potentials from 0.1 to –0.5 V vs Ag/AgCl. The corresponding phase angle plots are shown in Figure 1B. For potentials between 0.1 and –0.1 V vs Ag/AgCl, a plateau corresponding to phase angle ~80^{o} is observed. This value indicates that the impedance is primarily determined by the capacitance of the interface. At more negative potentials, the phase angles decrease significantly at frequencies below 1 Hz, which indicates an onset of channel or defect formation in the bilayer.

Figure S3 compares the impedance and phase angle spectra of the DPhPC fBLM with gA (red) and without gA (black) in 0.1 M NaF solution at an electrode potential of 0.0 V vs Ag/AgCl. The error bars in these measurements are small and demonstrate that the electrical differences between the two different films are real. These plots show that the magnitude of the impedance at $f < 100$ Hz is lower when gA is present in the membrane. Additionally, the phase angles are always smaller when gA is present. These two features suggest that gA forms ion channels in the DPhPC bilayer and Na^{+} could cross the membrane through these channels leading to the decrease of both the bilayer impedance and phase angle [32, 33].

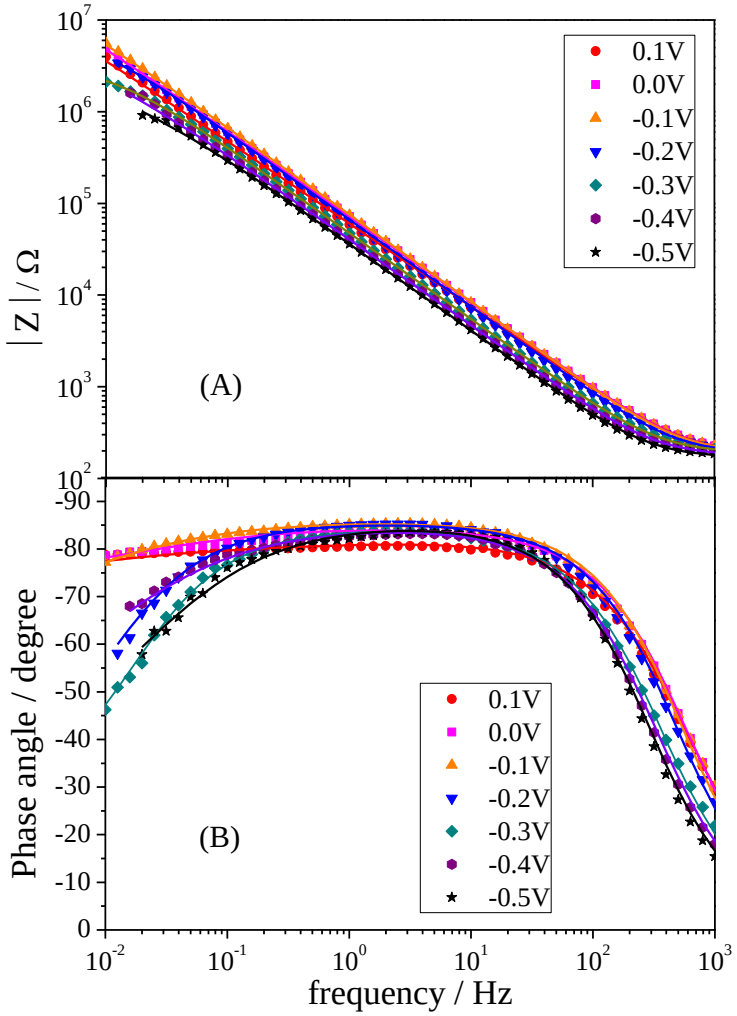

Figure 1 (A) Magnitude of the impedance and (B) phase angle plots obtained from the EIS spectra of the DPhPC/gA fBLM in 0.1 M NaF at different potentials. The symbols represent the experimentally collected data and the solid lines are the resulting fits using the equivalent circuit shown in Scheme 1.

To quantitatively describe the ion channel properties of gA, the impedance spectra of the DPhPC/gA fBLM were fit using the equivalent circuit shown in Scheme 1. This model, proposed by Valincius's group [34, 35], considers the diffusion of ions through channels (pores) in the membrane, which is separated from the metal surface by a water-rich region provided by the SAM of hydrophilic β-Tg. In this model, R_{sol} represents the solution

resistance, R_m and CPE_m are resistance and constant phase element (CPE) of the bilayer lipid membrane, respectively. CPE_{sp} corresponds to the constant phase element of the β-Tg spacer. The impedance of CPE is defined as:

$$Z_{CPE} = \frac{1}{Q(j\omega)^{\alpha}} \quad (1)$$

where Q is the constant phase element coefficient with the unit of μF cm^{-2} $s^{\alpha-1}$ and α is an empirical constant related to the frequency dispersion, whose value varies between 0 and 1. When α is close to 0, the impedance of CPE is close to the impedance of a resistor, and CPE represents a capacitor when α is close to 1.

Table 1 Numerical values of the equivalent circuit elements of the DPhPC/gA fBLM in 0.1 M NaF at different potentials.

E / V vs Ag/AgCl	Q_m / μF cm^{-2} $s^{\alpha-1}$	α_m	R_m / MΩ cm^2	Q_{sp} / μF cm^{-2} $s^{\alpha-1}$	α_{sp}
0.1	12.5 ± 1.3	0.910 ± 0.005	1.29 ± 0.25	0.63 ± 0.05	0.603 ± 0.052
0.0	10.4 ± 1.0	0.938 ± 0.004	1.91 ± 0.36	0.75 ± 0.09	0.525 ± 0.036
–0.1	9.6 ± 1.0	0.952 ± 0.006	1.68 ± 0.25	0.65 ± 0.13	0.465 ± 0.020
–0.2	10.9 ± 1.1	0.951 ± 0.006	1.39 ± 0.22	2.31 ± 0.3	0.487 ± 0.028
–0.3	13.9 ± 1.4	0.947 ± 0.006	0.71 ± 0.05	5.2 ± 0.7	0.432 ± 0.050
–0.4	18.3 ± 1.8	0.940 ± 0.007	0.29 ± 0.04	3.2 ± 0.3	0.397 ± 0.019
–0.5	18.7 ± 1.9	0.949 ± 0.008	0.15 ± 0.01	1.7 ± 0.3	0.311 ± 0.019

The numerical values of the equivalent circuit elements for the DPhPC/gA fBLM in 0.1 M NaF are listed in Table 1. At all potentials, the values of α_m are close to 1, indicating that the bilayer behaves as a capacitor, and the values of Q_m can be considered

as the capacitance of the interface. In contrast, the value of α_{sp} is around 0.5 in the potential region between 0.1 and –0.3 V vs Ag/AgCl. These numbers are characteristic of the Warburg impedance and suggest that the impedance of the β-Tg spacer is controlled by the diffusion of ions through channels or defects in the bilayer [34]. At the most negative potentials, the values of α_{sp} become smaller than 0.5 suggesting a more resistive character of the spacer region [34].

Figure 2A compares the variation of the membrane capacitance (Q_m) of the DPhPC fBLM with gA (red circles) and without gA (black triangles) as a function of the applied potential. The top horizontal axis plots E-E_{pzfc}, where E_{pzfc} is the potential of zero free charge on the gold electrode and the charge in the diffuse part of the double layer equals zero. The difference E-E_{pzfc} approximates the transmembrane potential across the DPhPC/gA fBLM. The value of E_{pzfc} was measured by the immersion method [36]. Figure S4 of SI plots the double layer charge density of the DPhPC/gA fBLM in 0.1 M NaF solution as a function of the immersion potential. The free charge density linearly increases with the electrode potential and displays a value of zero charge at the potential of 0.25 ± 0.03 V vs Ag/AgCl. E_{pzfc} of the fBLM without gA in the same supporting electrolyte is equal to 0.22 ± 0.02 V [25]. These numbers are equal within experimental uncertainty.

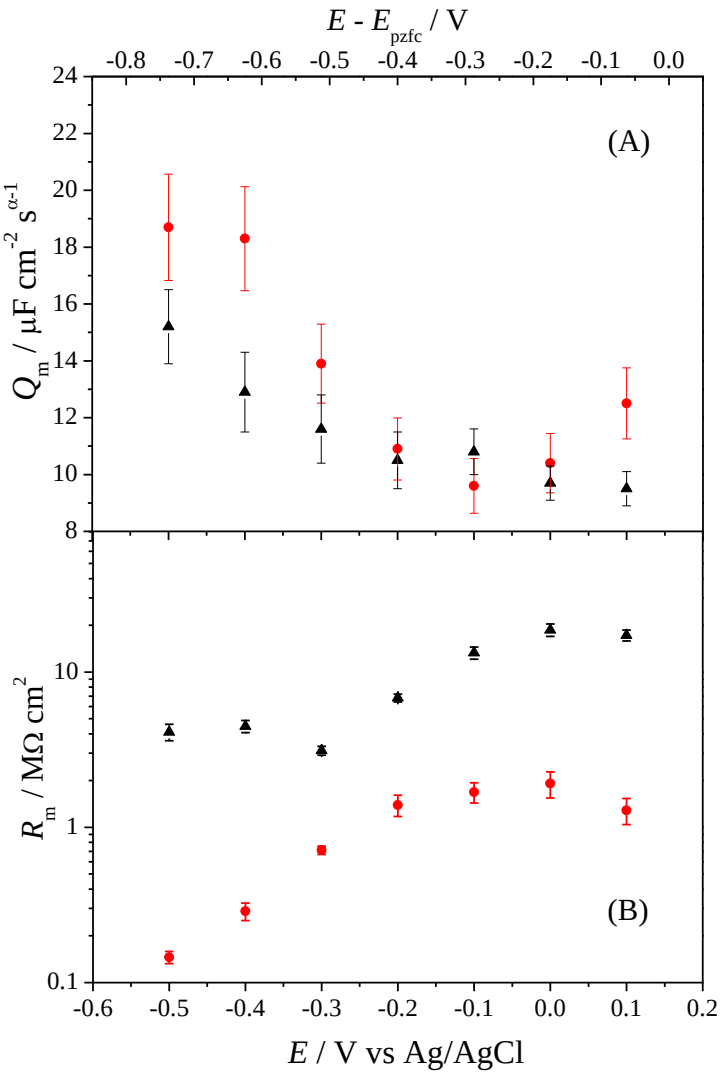

Figure 2 Variation of the (A) membrane capacitance (Q_m) and (B) membrane resistance (R_m) of the DPhPC fBLM with gA (red circles) and without gA (black triangles) in 0.1 M NaF as a function of potential. The data of the DPhPC fBLM was taken from Ref. [25].

The Q_m values of fBLMs in the absence and presence gA display a minimum of ~10 μF cm^{-2} at $E \approx -0.1$ V vs Ag/AgCl or E-$E_{pzfc} = -0.3$ V. The equivalent circuit in Scheme 1 shows that Q_m includes properties of the water-rich spacer layer, which explains its high value. The capacitance increases at $E \leq -0.3$ V vs Ag/AgCl indicating the onset of electroporation or electrodewetting of the membrane from the electrode surface. At $E \leq$

–0.3 V vs Ag/AgCl, the capacitance of the interface is higher in the presence of gA than in the absence of the peptide. This result suggests that water molecules are transported through gA channels [37] leading to a higher concentration of water in the interior region of the bilayer and larger capacitance of the interface.

Figure 2B compares the membrane resistance of the DPhPC fBLM with gA (red circles) and without gA (black rectangles) at different potentials. At all potentials, the resistance of the bilayer without gA is ~ 5 to 20 times larger than the resistance of the bilayer with gA. This result indicates that gA forms ion channels in the fBLM and that Na^+ is transported across the membrane decreasing its resistance [14]. The maximum values of R_m are observed around E = –0.1 V vs Ag/AgCl and correspond to the potential of minimum values of Q_m. The membrane resistance decreases at more negative potentials. The decrease is much more pronounced when gA is present in the membrane correlating well with a more pronounced increase of Q_m at these negative potentials.

Recent studies of ionophore properties of valinomycin, another antibiotic peptide, showed that the anion present in the electrolyte has a significant effect on the membrane resistivity of the DPhPC fBLM incorporated with valinomycin [15]. These studies showed that perchlorate, an anion with low hydration energy, facilitates the transport of potassium cation across the bilayer and has a significant impact on membrane resistivity. Therefore, the impedance spectra of the DPhPC/gA fBLM were also measured in 0.1 M $NaClO_4$ solution, to check if the conductivity of Na^+ through gA channels is also assisted by the counterion. The free energy of ClO_4^- hydration amounts to -205 kJ mol^{-1} while the energy of hydration of F^- is equal to -465 kJ mol^{-1} [28]. The differences between the hydration energies of the two anions are large. The impedance data of gA in $NaClO_4$ are shown in Figure S5 of SI. The impedance spectra of gA in $NaClO_4$ solution are similar to those in

NaF solution. The EIS data of gA in 0.1 M $NaClO_4$ were fitted using the same equivalent circuit shown in Scheme 1. The elements of the equivalent circuit obtained from the fit are listed in Table S1 of SI. At all potentials, the values of α_m are close to 1, demonstrating that the bilayer behaves as a capacitor on the gold surface, and the values of Q_m can be treated as the capacitance of the interface.

To compare the ion channel properties of gA in the DPhPC fBLM in the two electrolytes, Figure 3A plots the capacitance of the DPhPC/gA fBLM in NaF and $NaClO_4$ solutions. Additionally, Figure 3B compares the corresponding values of the membrane resistance. Within experimental errors, the values of capacitance and membrane resistance are independent of the nature of the anion. This result shows that despite a large difference in the solvation energies of the F^- and ClO_4^- anions, they do not influence the structure of the bilayer and sodium cation transport across gA channels.

This behavior is contradictory to the properties of valinomycin where potassium cation is transported across the membrane as an ion pair with the counter anion of the supporting electrolyte [15, 38]. This is also in contrast to the channel properties of gA in a free-standing black lipid membrane (BLM). Shirai et al. studied the ion channel properties of gA in a BLM in electrolytes containing different anions [17]. They found that the conductivity of gA channels increased with the decrease of the hydration energy of the counter anion in the supporting electrolyte. When sodium cations are transported through a channel in a free-standing bilayer (BLM), the concomitant transport of the counterion prevents the buildup of charge across the membrane. In the case of fBLM, the positive charge of Na^+ transported to the spacer layer is compensated by the negative charge flowing to the metal side of the interface.

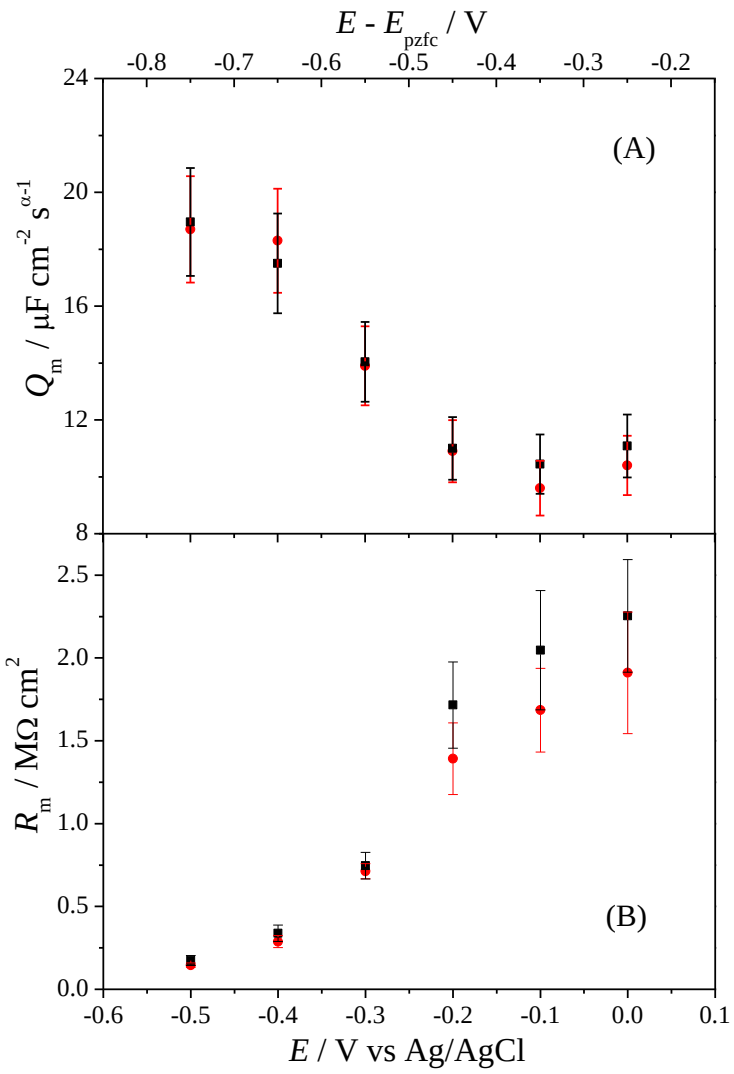

Figure 3 Variation of the (A) membrane capacitance (Q_m) and (B) membrane resistance (R_m) of the DPhPC/gA fBLM in 0.1 M NaF (red circles) and 0.1 M $NaClO_4$ (black rectangles) as a function of potential.

Despite the lack of anion effects on the membrane properties, the anions do affect the properties of the spacer layer. Figure 4 plots the values of Q_{sp} and α_{sp} for fBLMs in the two electrolytes versus the electrode potential. For $E > -0.2$ V vs Ag/AgCl, the values of Q_{sp} for two electrolytes are small (less than 1 μF cm^{-2}) and $\alpha_{sp} \approx 0.5$. These values indicate that the impedance of the spacer layer is high and is controlled by the transport of sodium

cations through the ion channels. However, at $E < -0.2$ V vs Ag/AgCl the values of Q_{sp} become much higher and α_{sp} is lower in the $NaClO_4$ solution. This behavior indicates that the impedance of the spacer layer becomes smaller in the presence of fluorides than in the presence of perchlorates. The Q_{sp} displays a maximum at E~-0.3V vs Ag/AgCl. The increase in Q_m and decrease in R_m (see Figure 3) indicates the onset of electrodewetting of the membrane from the gold surface. This has been confirmed by neutron reflectivity, which demonstrated that the membrane swells and becomes leaking when electrodewetting takes place [39]. The values of α_{sp} become much lower than 0.5 at E<-0.3 v vs Ag/AgCl indicating that the impedance of the spacer layer has a resistive character. This behavior is consistent with the electroporation of the membrane. When pores are formed in the membrane, both sodium cations and anions enter into the spacer layer. The impedance of the spacer layer becomes controlled by the ionic conductivity. The data suggest that more hydrated fluorides are more easily transported through the water-filled pores in the membrane and hence have a stronger effect on the electrical properties of the spacer layer.

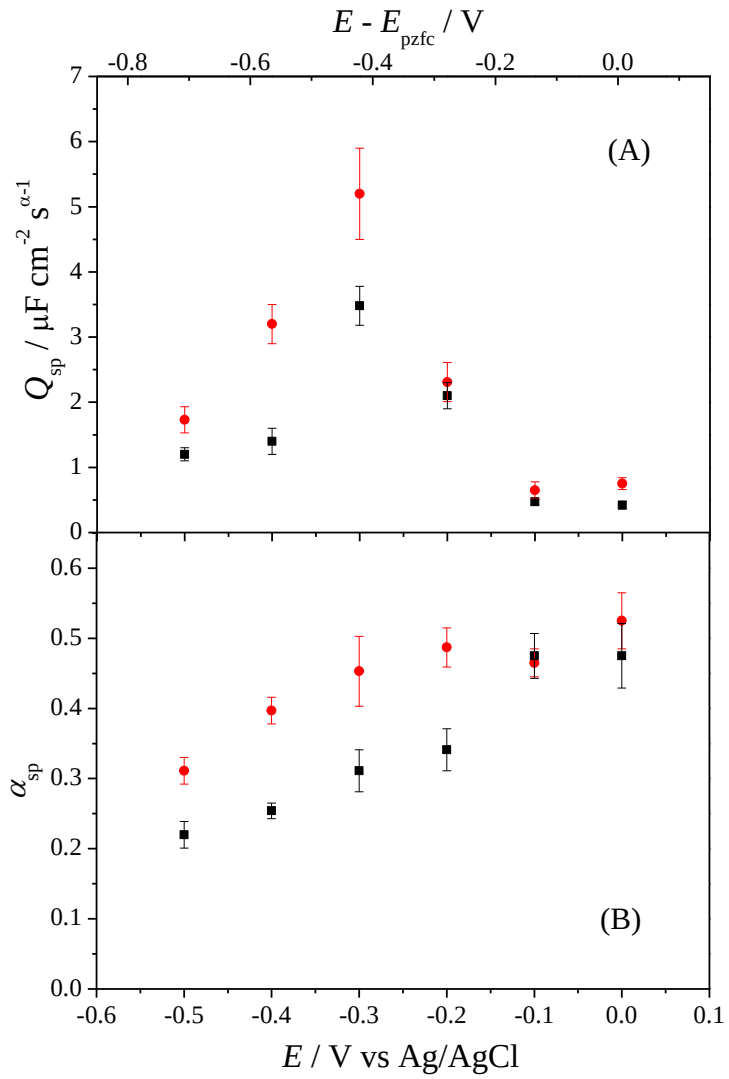

Figure 4. Variation of (A) Q_{sp} and (B) α_{sp} of the DPhPC/gA fBLM in 0.1 M NaF (red circles) and 0.1 M $NaClO_4$ (black rectangles) as a function of potential.

The electrochemical data show that gA behaves as an ion channel in the fBLM, both in NaF and $NaClO_4$ solutions. In the next section, the in situ PM-IRRAS technique was employed to provide molecular-level information concerning the conformation and orientation of gA in the fBLM in two supporting electrolytes.

3.2 Infrared characterization

3.2.1 C=O and Amide I bands region

Figure 5 shows the PM-IRRAS spectra of the C=O stretching and amide I vibrations of the DPhPC/gA fBLM in 0.1 M NaF/D_2O solution. The IR band between 1600 and 1700 cm^{-1} corresponds to the amide I absorption of gA [9, 11, 13] and the band between 1700 and 1760 cm^{-1} is assigned to the C=O stretching from the ester moiety of DPhPC molecules [40]. The intensity of the ester C=O band is nearly potential independent, while the intensity of the gA amide I band increases when the electrode potential becomes more negative. This result suggests that the orientation of DPhPC does not change with potential despite changes in the orientation of the gA peptides within the film.

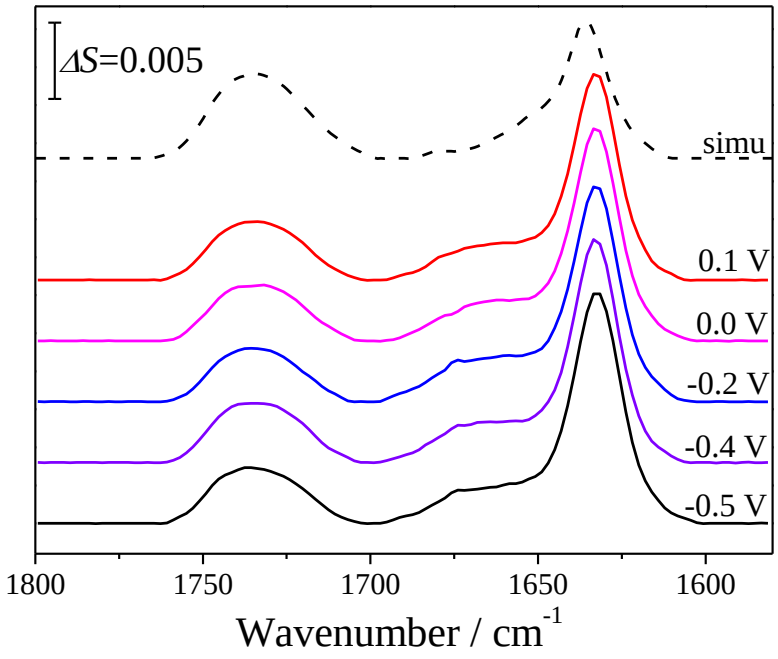

Figure 5 PM-IRRAS spectra showing the C=O stretching and amide I regions of the DPhPC/gA fBLM in 0.1 M NaF/D_2O at selected potentials. The top dashed line represents the simulated IR spectrum of a random oriented DPhPC/gA fBLM. The bilayer was transferred using the LB-LS technique at a film pressure of 28 mN m^{-1}.

The amide I band of gA is a broad band containing several sub-bands corresponding

to different secondary structures. The Fourier self-deconvolution (FSD) and second derivative (SD) techniques were employed to assist the band deconvolution. Figure 6A plots the FSD and SD analysis of the amide I spectrum at $E = 0.0$ V vs Ag/AgCl. The strong band around 1633 cm^{-1} is assigned to the β-helix dimer ($\beta^{6.3}$-helix) of gA [11, 13, 14, 41]. There are also six small bands at 1618, 1647, 1655, 1662, 1669 and 1680 cm^{-1} attributed to the double helix ($\beta^{5.6}$-helix) conformation of gA [11, 13, 14, 41]. Figure 6B displays the deconvolution of the IR spectrum in the amide I region at $E = 0.0$ V vs Ag/AgCl. The percentage of the area under the $\beta^{6.3}$-helical dimer band is ~61% of the total area of the amide I band, indicating that $\beta^{6.3}$-helical dimer is the predominant secondary structure of gA in the fBLM.

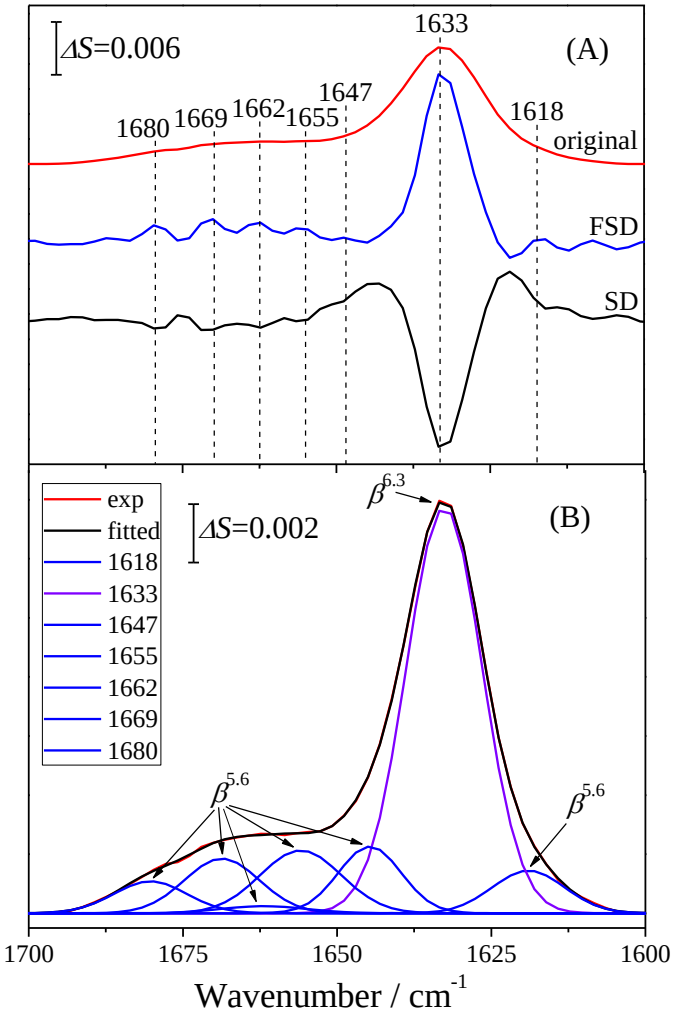

Figure 6 (A) Fourier-self deconvolution and second derivative results for the PM-IRRAS spectrum of the DPhPC/gA fBLM in 0.1 M NaF/D_2O at E=0.0 V. (B) Deconvolution of the PM-IRRAS spectrum of the DPhPC/gA fBLM in the amide I region at E=0.0 V.

However, the relative presence of the $\beta^{6.3}$ and $\beta^{5.6}$ conformers depends on the surface pressure at which the two leaflets were transferred from the air-solution interface using the LB-LS procedure. Figure 7A shows PM-IRRAS spectra recorded when the bilayer was transferred onto the gold electrode by compressing the LB film to 35 mN m^{-1}. The electrode was first brought in contact with the electrolyte at E = 0.1 V vs Ag/AgCl and then the potential was progressively moved in the negative direction. The shapes of these

spectra indicate that the amide I band is dominated by the $\beta^{5.6}$ conformation for all positive potentials prior to $E = -0.6$ V vs Ag/AgCl. At more negative potentials, the bilayer detaches from the electrode surface. The final two recorded spectra in the series show that the amide I band once again becomes dominated by the $\beta^{6.3}$ conformation in the detached state.

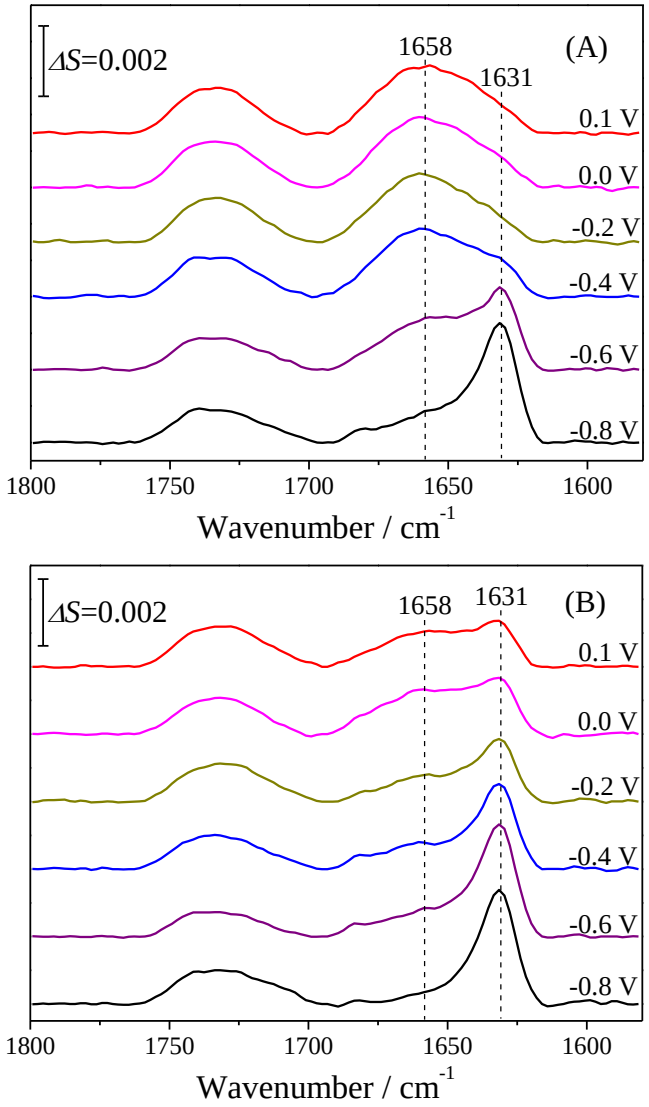

Figure 7. PM-IRRAS spectra of the DPhPC/gA fBLM in the C=O stretching and amide I region at different electrode potentials. The bilayer was transferred using the LB-LS technique at a film pressure of 35 mN m^{-1}. The spectra shown in (A) were recorded after contacting the electrode with 0.1 M NaF/D_2O electrolyte at $E = 0.1$ V vs Ag/AgCl and the scanning to negative potentials. The spectra in (B) were recorded after the bilayer was

desorbed from the electrode surface at E = -1.0 V vs Ag/AgCl and redeposited during the positive potential scan.

When the direction of the potential change is reversed and the spectra are recorded by moving potential back in the positive direction (see Figure 7B), the shape of the amide I band suggests that the $\beta^{6.3}$ conformer is dominant even at potentials where the bilayer is redeposited onto the electrode surface.

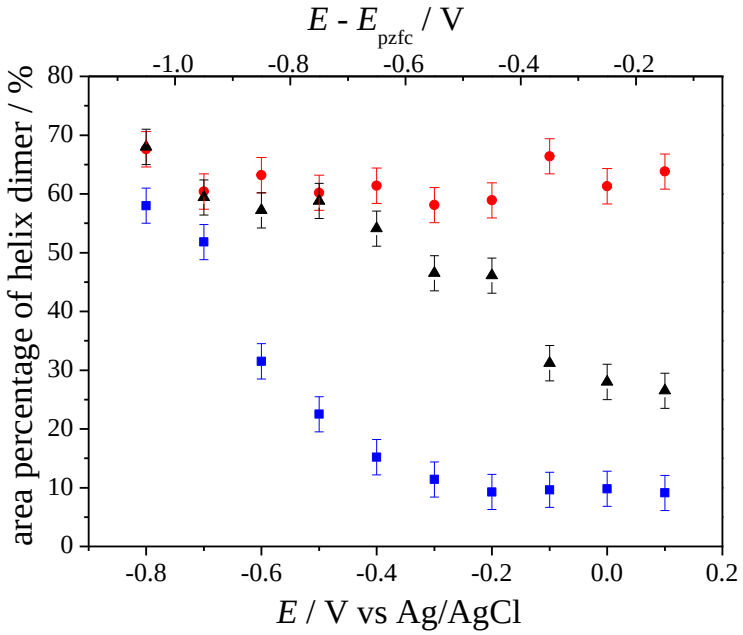

Figure 8. Percentage of the helical dimer conformer (1633 cm^{-1} band) in the amide I region showing the fBLM formed by transfer monolayers at film pressure 28 mN m^{-1}(red circles); at 35 mN m^{-1} for the negative potential scan (blue squares); at 35 mN m^{-1} for the positive potential scan (black triangles).

The spectra in Figure 5 and Figures 7A and B were deconvoluted and the area of the $\beta^{6.3}$-helical dimer band at 1633 cm^{-1} was calculated. The ratio of the area corresponding to $\beta^{6.3}$ band to the total area of the amide I band was determined and plotted as a percentage of the $\beta^{6.3}$ conformer within the bilayer in Figure 8. The data shows that the content of the

$\beta^{6.3}$ conformer in the bilayer formed by transferring monolayers at 28 mN m^{-1} is ~61 % independently of the applied potential. However, when the bilayer is formed by transferring monolayers at 35 mN m^{-1}, the content of the $\beta^{6.3}$ conformer is much lower at the initial positive potentials and reaches ~ 60% at the most negative potentials. When the bilayer was brought in contact at 0.1 V vs Ag/AgCl, the $\beta^{6.3}$ conformer amounts to ~10% and only increases after detachment of the bilayer at $E < -0.4$ V vs Ag/AgCl. For the bilayer reformed at the electrode surface by moving potential back in the positive direction, the content of the $\beta^{6.3}$ conformer drops down to ~30 % when the bilayer reestablishes contact with the electrode surface. The $\beta^{6.3}$ conformer has a larger cross-sectional area than the $\beta^{5.6}$ form. Therefore, present data show that high film pressure shifts the equilibrium between the two conformers causing the gA molecules to adopt the $\beta^{5.6}$ structure since it occupies a smaller area per molecule. This result is consistent with studies of the effect of pressure and temperature on the equilibrium between $\beta^{6.3}$ and $\beta^{5.6}$ conformers in a suspension of phospholipid vesicles containing gramicidin by Zein and Winter [42]. They showed that the equilibrium is shifted towards the formation of the $\beta^{5.6}$ conformer at higher pressures. Similar behavior is observed in 3D and 2D systems.

The area of the 1633 cm^{-1} band could be used to calculate the orientation of the $\beta^{6.3}$-helix (average tilt angle between the helix axis and the surface normal, γ_{helix}). The procedure used to calculate γ_{helix} is described in the Supporting Information. The tilt angle of the $\beta^{6.3}$ helix is an average value of all orientations of $\beta^{6.3}$ helix incorporated into the fBLM. A small value of γ_{helix} demonstrates $\beta^{6.3}$ helices are inserted into the fBLM.

Figure 9 plots the variation of γ_{helix} in the DPhPC fBLM in 0.1 M NaF solution (red circles) as a function of the applied potential. At positive transmembrane potentials, the average tilt angle of $\beta^{6.3}$-helix is ~30°. When the transmembrane potential becomes more

negative, the value of γ_{helix} becomes smaller. At the electrode potential of 0.0 V or E-E_{pzfc} = –0.25 V, γ_{helix} equals ~29°, and this value decreases to ~24° at E-E_{pzfc} = –0.75 V. This trend correlates well with the EIS data in Figure 2 that show a decrease in the membrane resistance of the DPhPC/gA bilayer when E-E_{pzfc} becomes more negative. The decrease of the tilt angle may indicate an increase in the population of inserted gA and an increase in the density of $\beta^{6.3}$ channels. In the double layer region, the values of γ_{helix} of gA in the DPhPC fBLM are similar to that in the DPhPC/DPTL tBLM, which displayed a helical angle of 29 ± 3° [14] indicating the orientation of gA in the fBLM and tBLM is similar.

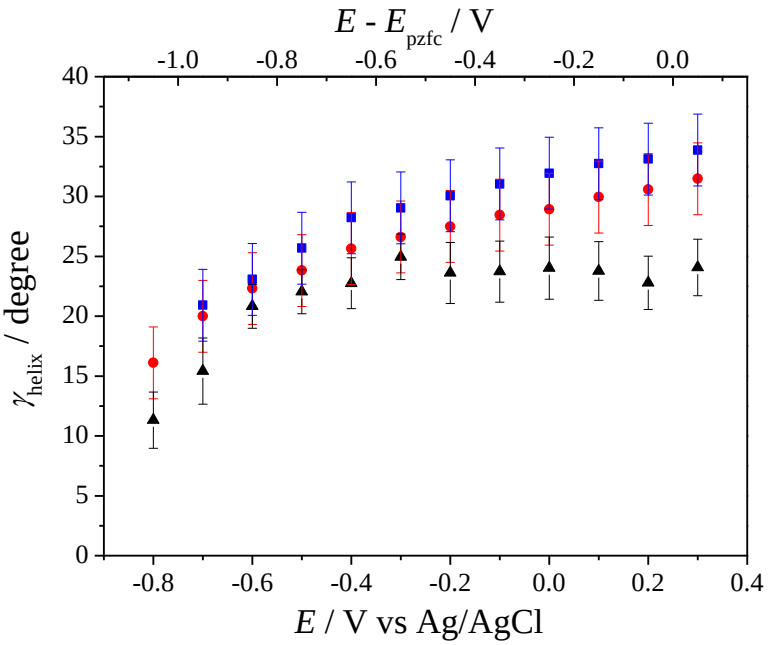

Figure 9 Variation of the average tilt angle of gA in the DPhPC fBLM in 0.1 M NaF/D_2O (red circles) and 0.1 M $NaClO_4/D_2O$ (blue rectangles) as a function of the potential. The black triangles display the average tilt angle of gA in the sBLM in 0.1 M NaF taken from Ref. [13].

The orientation of $\beta^{6.3}$-helix of gA in the sBLM directly deposited at the electrode surface, not modified by β-Tg monolayer, is plotted in Figure 9 as the black triangles (data

were taken from Ref. [13]). The values of γ_{helix} in the sBLM are constant and approximately equal to ~24°, at potentials between 0.3 and –0.3 V vs Ag/AgCl, where the bilayer is in direct contact with the metal. The orientation of $\beta^{6.3}$-helix does not change with potential in this region. The average tilt angle of $\beta^{6.3}$-helix rapidly decreases at $E < -0.3$ V, where electroporation and electrodewetting of the film take place. Additionally, the tilt angles of $\beta^{6.3}$-helix of gA in the sBLM are smaller than that in the fBLM.

To complement the EIS data, the PM-IRRAS spectra were recorded in 0.1 M $NaClO_4/D_2O$ supporting electrolyte. The PM-IRRAS spectra of the DPhPC/gA bilayer in the C=O stretching and amide I regions are shown in Figure S6 of SI. Besides, Figure S7 of SI shows a comparison of the spectra recorded in 0.1 M NaF and 0.1 M $NaClO_4$. The spectra were divided by the surface enhancement factor to remove differences in the optical setup (see Equation S2 of SI). The spectra recorded in the two electrolytes are quite similar. The deconvolution of the amide I band of gA in $NaClO_4$ solution is presented in Figure S8. The area percentage of the $\beta^{6.3}$-helix band is ~54%, suggesting that is $\beta^{6.3}$-helix is the predominant structure of gA in the fBLM in the $NaClO_4$ solution. Figure S9 of SI compares the percentage of the $\beta^{6.3}$-helix band in fBLM for 0.1 M NaF and 0.1 M $NaClO_4$ solutions. The content of $\beta^{6.3}$-helix is independent of the electrode potential and is about 5% lower in the perchlorate solution. This result is consistent with somewhat higher membrane resistance in 0.1 M $NaClO_4$ solution. Figure 9 shows that changes of the tilt angle of $\beta^{6.3}$-helix with potential are similar in the two electrolytes. The γ_{helix} values are about 2° higher in the 0.1 M $NaClO_4$ solution, but these differences are within the experimental errors.

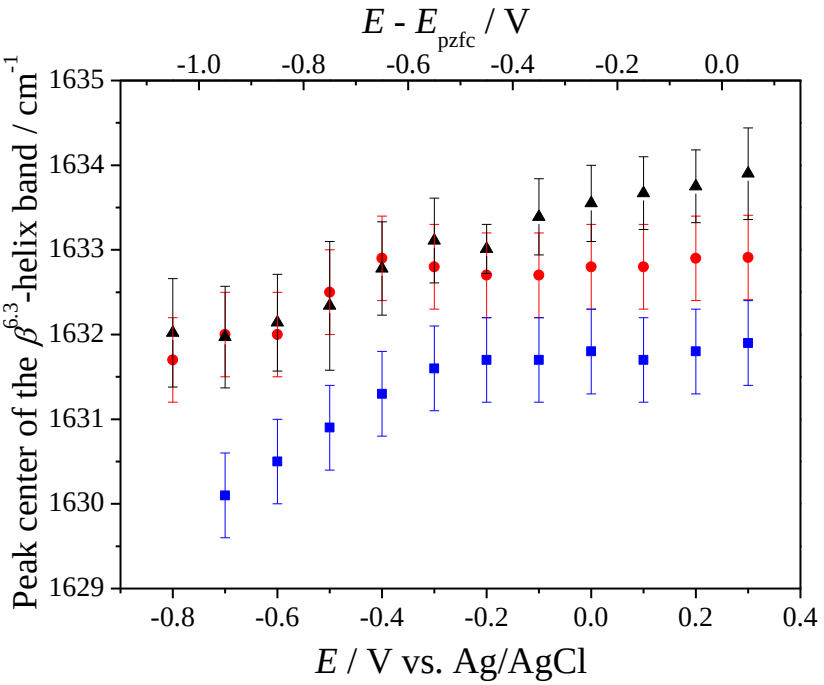

Figure 10. Variations in the $\beta^{6.3}$-helix band peak center of the DPhPC/gA fBLM in 0.1 M NaF/D_2O (red circles) and 0.1 M $NaClO_4/D_2O$ (blue squares) as a function of the potential. The black triangles display the peak center variations of the $\beta^{6.3}$-helix band in the sBLM in 0.1 M NaF/D_2O taken from Ref. [13].

The peak position of the amide I band depends on the strength of intramolecular hydrogen bonds and the transition dipole coupling (TDC) [43], which determine the stability of the given element of the secondary structure of the peptide. Figure 10 plots the $\beta^{6.3}$-helix band position in three bilayers. The highest frequencies of the band position are observed for the sBLM in 0.1 M NaF and the lowest for fBLM in the $NaClO_4$ solution. For the fBLM in the NaF electrolyte, the band centers are located in between these two extremes. For all three bilayers, the band centers decrease at $E < -0.4$V vs Ag/AgCl where the bilayers are detached from the metal surface. A shift to lower wavenumbers indicates stronger intramolecular hydrogen bonds and stronger transition dipole coupling. The strength of TDC depends on the distance and relative orientation of the vibrating dipoles.

The lower wavenumber of the peak center of the amide I band suggests stronger TDC and/or intramolecular hydrogen bonds. The position of the $\beta^{6.3}$ band center in the fBLM is lower than that of the sBLM indicating that gA is less stressed in the fBLM than in the sBLM. The hydrated β-Tg monolayer separates the bilayer from the gold surface in fBLM releasing the stress in the bilayer. In the sBLM, the bilayer is directly deposited on the gold surface. The stress increases when the lipid and peptides contact the substrate in sBLM. At potentials $E \leq -0.4$ V vs Ag/AgCl the bilayers are lifted and are separated from the metal surface by a cushion of electrolyte [39]. The bilayers are exposed to a more symmetric environment. The red shift of the band center demonstrates that the stress is then further released. Figure S10 of SI compares the $\beta^{6.3}$-helix band positions in the fBLM and tBLM (data taken from Ref. [14]). The spectra for the two bilayers were measured in 0.1 M perchlorate solution. In fBLM, the bilayer is floating on a water-rich β-Tg monolayer modified gold surface, while in the tBLM, the bilayer is separated from the metal by a tether of tetraethylene glycol subunits. The $\beta^{6.3}$-helix band positions are red shifted in the fBLM relative to the tBLM and indicates that more water is present in the spacer layer of the fBLM.

3.2.2 C-H stretching region

The C-H stretching region of PM-IRRAS spectra of the DPhPC/gA bilayer in 0.1 M NaF/D_2O is shown in Figure S11A. The spectra are similar to those reported in Ref. [14] and [44]. The procedure described in Ref. [44] was used to assist the band deconvolution of the spectrum plotted in Figure S11B. The spectrum is composed of bands from the CH_2 symmetrical ($\nu_s(CH_2)$) and asymmetrical ($\nu_{as}(CH_2)$) stretching, CH_3 symmetrical ($\nu_s(CH_3)$)

and asymmetrical ($\nu_{as}(CH_3)$) stretching and C-H stretching ($\nu(CH)$). The peak centers of the $\nu_s(CH_2)$ and $\nu_{as}(CH_2)$ bands are located at 2958 ± 1 and 2927 ± 1 cm^{-1}. These values are higher than those in a gel state of fully stretched acyl chains [45], indicating that DPhPC molecules are in the liquid crystal state in the DPhPC/gA bilayer.

The integrated intensities of $\nu_s(CH_2)$ and $\nu_{as}(CH_2)$ bands can be used to calculate the average orientation of trans fragments of diphytanoyl chains with respect to the surface normal (θ_{chain}) using the procedure described both in Ref. [44] and the Supporting Information. Figure 11 plots θ_{chain} of the DPhPC bilayer with gA (red circles) and without gA (black triangles) in 0.1 M NaF/D_2O solution as a function of applied potential. Within the experimental uncertainties, the θ_{chain} of DPhPC molecules is potential independent. In the presence of gA, the angle is 33 ± 3°. This value is ~4° higher than θ_{chain} in the DPhPC bilayer without gA[25] indicating that gA causes thinning of the bilayer. A similar trend was observed for gA incorporated into the sBLM [13] and tBLM [14]. The outer surface of the gA channel is hydrophobic. The energetics requires that the length of the channel projected onto the surface normal matches the hydrophobic thickness of the bilayer [46]. The length of the $\beta^{6.3}$-helical dimer is equal to 2.6 nm [47]. The average tilt angle of the $\beta^{6.3}$-helix structure of gA in the double layer region is ~ 29 ± 3°. Hence the projected length of the helical dimer onto the surface normal equals 2.3 ± 0.1 nm. In the absence of gA, the thickness of the hydrophobic region of the DPhPC bilayer is around 2.7 nm [48]. This value is ~0.4 nm larger than the projected length of gA channel onto the surface normal. To reduce the hydrophobic mismatch between the hydrophobic region of the bilayer and the projected length of gA channels, DPhPC molecules are more tilted in the bilayer with gA [46].

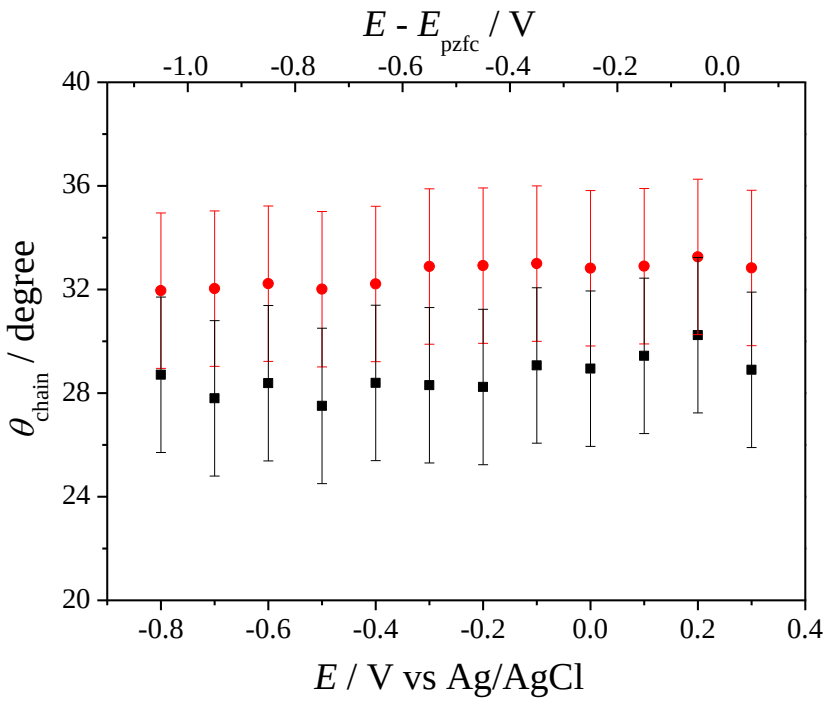

Figure 11 Variation of the average tilt angle of DPhPC in the fBLM with gA (red circles) and without gA (black triangle) in 0.1 M NaF/D_2O as a function of the potential. The data of the fBLM without gA was taken from Ref. [25].

4. Conclusion

EIS and PM-IRRAS techniques were employed to study the ion channel properties of gA in the DPhPC floating bilayer. There are several notable results of these studies. (i) They demonstrate that the surface pressure of the bilayer has a significant impact on the relative distribution of the channel forming $\beta^{6.3}$ double helix and pore forming $\beta^{5.6}$ conformer. (ii) They show that the nature of the anion in the supporting electrolyte has a negligible effect on the transport of sodium cation through the gA channel incorporated into the floating bilayer of DPhPC. Table 2 illustrates that the membrane resistance, the average tilt angle of $\beta^{6.3}$ helix, the content of $\beta^{6.3}$ helix, and the position of $\beta^{6.3}$ helix band in the IR spectrum of a floating DPhPC bilayer are within experimental uncertainties

between the supporting electrolyte containing 0.1 M NaF and 0.1 M $NaClO_4$ despite significant differences between hydration energies of fluoride and perchlorate. (iii) These studies demonstrate that the membrane resistance and hence ion channel conductivity depends on the transmembrane potential. This point is illustrated in Figure 12, which plots the logarithm of conductivity ($1/R_m$) as a function of (E-E_{pzfc}-ϕ_{OHP}) for the region where the membrane is stable at the electrode surface. For comparison, the change of the $\beta^{6.3}$ helix tilt angle is also plotted in this figure. The conductivity increases when the potential moves in the negative direction. This change is to some degree correlated with a decrease of the $\beta^{6.3}$ helix tilt angle. Interestingly, the logarithm of conductivity changes linearly with potential within the range from –0.1 to –0.5 V vs Ag/AgCl. This relation suggests that:

$$\frac{1}{R_m} \propto e^{-\frac{\alpha F(E-E_{\mathrm{pzfc}})}{RT}} \qquad (2)$$

with the slope corresponding to $\alpha = 0.2$. The coefficient α represents the fraction of the potential difference metal-solution interphase that affects the ion-transfer step [49]:

$$\alpha = \frac{\varphi^* - \varphi_s}{\varphi_m - \varphi_s} \qquad (3)$$

here φ^* is the potential on the location of the ion transfer rate determining step, φ_m is the potential on the metal surface and φ_s is the potential on the solution side of the interface. The value of $\alpha = 0.2$ suggests that the rate-determining step is located far away from the metal surface at a point where only 20% of the applied potential difference is acting on the ion. The thickness of the floating bilayer is estimated to be ~5 nm [50]. Consequently, the value $\alpha = 0.2$ indicates that the location of the rate determining state is ~1 nm from the top of the bilayer and in the middle of its first leaflet. Figure 12 also shows that the increase of conductivity with negative transmembrane potential correlates with a decrease of the tilt angle of the $\beta^{6.3}$-helix. The decrease of the tilt angle is a manifestation of better

hydrophobic matching and hence increased stability of the ion channel. Consequently, this result provides significant molecular-level data in support of models developed by Bamberg and Lauger [51] and Becucci et al. [21] which assume increased gA dimer concentration at more negative transmembrane potentials.

Table 2 Comparison DPhPC/gA fBLM parameters in 0.1 M NaF and 0.1 M $NaClO_4$ at E = 0.0 V.

Supporting electrolyte	R_m / MΩ m^2	γ_{helix} /degree	$\beta^{6.3}$ %	Peak center of the $\beta^{6.3}$-helix band / cm^{-1}
NaF	1.91 ± 0.36	29 ± 3	61 ± 3%	1633 ± 1
$NaClO_4$	2.25 ± 0.34	32 ± 3	54 ± 3%	1632 ± 1

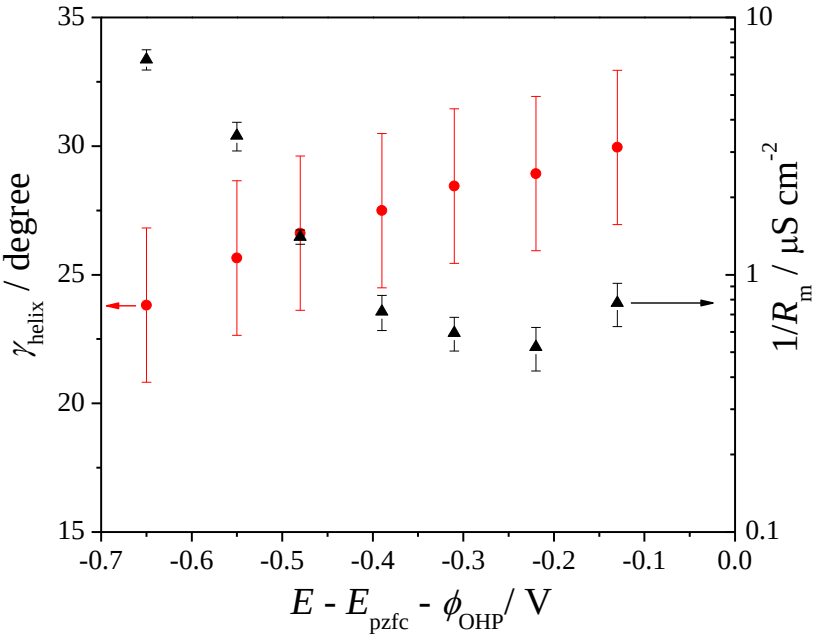

Figure 12. Variation of the average tilt angle of gA (left y-axis) and membrane conductance ($1/R_m$, right y-axis) of the DPhPC/gA fBLM in 0.1 M NaF as a function of the transmembrane potential.

Acknowledgements

This work was supported by a grant from the Natural Sciences and Engineering Research Council of Canada (NSERC) to JL (RG-03958).

Supporting Information

Supporting information associated with this article can be found in the online version.

References:

[1] R. Reiter, E. Zaitseva, G. Baaken, I. Halimeh, J.C. Behrends, A. Zumbuehl, Activity of the Gramicidin A ion channel in a lipid membrane with switchable physical properties, Langmuir, 35 (2019) 14959-14966.

[2] T. Yamaguchi, Y. Kitazumi, K. Kano, O. Shirai, Permselectivity of Gramicidin A Channels Based on Single‐channel Recordings, Electroanalysis, 32 (2020) 1093-1099.

[3] B. Wallace, Gramicidin channels and pores, Annu. Rev. Biophys. Biophys. Chem., 19 (1990) 127-157.

[4] D.A. Kelkar, A. Chattopadhyay, The gramicidin ion channel: a model membrane protein, Biochim. Biophys. Acta, 1768 (2007) 2011-2025.

[5] J. Paulino, M. Yi, I. Hung, Z. Gan, X. Wang, E.Y. Chekmenev, H.-X. Zhou, T.A. Cross, Functional stability of water wire–carbonyl interactions in an ion channel, Proc. Natl. Acad. Sci. U. S. A., 117 (2020) 11908-11915.

[6] T.G. Meikle, C.E. Conn, F. Separovic, C.J. Drummond, Exploring the structural relationship between encapsulated antimicrobial peptides and the bilayer membrane mimetic lipidic cubic phase: studies with gramicidin A', RSC Adv., 6 (2016) 68685-68694.

[7] D. Sun, T.A. Peyear, W.D. Bennett, O.S. Andersen, F.C. Lightstone, H.I. Ingólfsson, Molecular mechanism for gramicidin dimerization and dissociation in bilayers of different thickness, Biophys. J., 117 (2019) 1831-1844.

[8] D. Langs, G. Smith, C. Courseille, G. Precigoux, Monoclinic uncomplexed double-stranded, antiparallel, left-handed beta 5.6-helix (increases decreases beta 5.6) structure of gramicidin A: alternate patterns of helical association and deformation, Proc. Natl. Acad. Sci. U. S. A., 88 (1991) 5345-5349.

[9] Z. Kóta, T. Páli, D. Marsh, Orientation and lipid-peptide interactions of gramicidin A in lipid membranes: polarized attenuated total reflection infrared spectroscopy and spin-label electron spin resonance, Biophys. J., 86 (2004) 1521-1531.

[10] P. Stevenson, A. Tokmakoff, Time-resolved measurements of an ion channel conformational change driven by a membrane phase transition, Proc. Natl. Acad. Sci. U. S. A., 114 (2017) 10840-10845.

[11] V.M. Naik, S. Krimm, Vibrational analysis of the structure of gramicidin AI Normal mode analysis, Biophys. J., 49 (1986) 1131-1145.
[12] J. Kozuch, C. Steinem, P. Hildebrandt, D. Millo, Combined Electrochemistry and Surface‐Enhanced Infrared Absorption Spectroscopy of Gramicidin A Incorporated into Tethered Bilayer Lipid Membranes, Angew. Chem. Int. Ed., 51 (2012) 8114-8117.
[13] T. Laredo, J.R. Dutcher, J. Lipkowski, Electric field driven changes of a gramicidin containing lipid bilayer supported on a Au (111) surface, Langmuir, 27 (2011) 10072-10087.
[14] Z. Su, J.J. Leitch, R.J. Faragher, A.L. Schwan, J. Lipkowski, Gramicidin A ion channel formation in model phospholipid bilayers tethered to gold (111) electrode surfaces, Electrochim. Acta, 243 (2017) 364-373.
[15] Z. Su, X. Ran, J.J. Leitch, A.L. Schwan, R. Faragher, J. Lipkowski, How Valinomycin Ionophores Enter and Transport K+ across Model Lipid Bilayer Membranes, Langmuir, 35 (2019) 16935-16943.
[16] Z. Su, D. Mrdenovic, S. Sek, J. Lipkowski, Ionophore properties of valinomycin in the model bilayer lipid membrane 1. Selectivity towards a cation, J. Solid State Chem., 24 (2020) 3125-3134.
[17] O. Shirai, Y. Yoshida, S. Kihara, T. Ohnuki, A. Uehara, H. Yamana, Ion transport across a bilayer lipid membrane facilitated by gramicidin A–Effect of counter anions on the cation transport, J. Electroanal. Chem., 595 (2006) 53-59.
[18] C. Steinem, A. Janshoff, H.-J. Galla, M. Sieber, Impedance analysis of ion transport through gramicidin channels incorporated in solid supported lipid bilayers, Bioelectrochem. Bioenerg, 42 (1997) 213-220.
[19] M. Naumowicz, Z. Figaszewski, Impedance analysis of phosphatidylcholine membranes modified with gramicidin D, Bioelectrochemistry, 61 (2003) 21-27.
[20] L. Becucci, R. Guidelli, Can gramicidin ion channel affect the dipole potential of neighboring phospholipid headgroups?, Bioelectrochemistry, 106 (2015) 343-352.
[21] L. Becucci, A. Santucci, R. Guidelli, Gramicidin conducting dimers in lipid bilayers are stabilized by single-file ionic flux along them, J. Phys. Chem. B, 111 (2007) 9814-9820.
[22] A.H. Kycia, S. Sek, Z. Su, A.R. Merrill, J. Lipkowski, Electrochemical and STM studies of 1-thio-β-d-glucose self-assembled on a Au (111) electrode surface, Langmuir, 27 (2011) 13383-13389.
[23] A.H. Kycia, J. Wang, A.R. Merrill, J. Lipkowski, Atomic force microscopy studies of a floating-bilayer lipid membrane on a Au (111) surface modified with a hydrophilic monolayer, Langmuir, 27 (2011) 10867-10877.
[24] Z. Su, J. Juhaniewicz-Debinska, S. Sek, J. Lipkowski, Water structure in the sub-membrane region of a floating lipid bilayer-the effect of an ion-channel formation and the channel blocker, Langmuir, 36 (2020) 409-418.
[25] Z. Su, M. Shodiev, J.J. Leitch, F. Abbasi, J. Lipkowski, Role of Transmembrane Potential and Defects on the Permeabilization of Lipid Bilayers by Alamethicin, an Ion-Channel-Forming Peptide, Langmuir, 34 (2018) 6249-6260.

[26] P. Pieta, M. Majewska, Z. Su, M. Grossutti, B. Wladyka, M. Piejko, J. Lipkowski, P. Mak, Physicochemical studies on orientation and conformation of a new bacteriocin BacSp222 in a planar phospholipid bilayer, Langmuir, 32 (2016) 5653-5662.

[27] J. Juhaniewicz-Debinska, D. Dziubak, S. Sek, Physicochemical Characterization of Daptomycin Interaction with Negatively Charged Lipid Membranes, Langmuir, 36 (2020) 5324-5335.

[28] Y. Marcus, Thermodynamics of solvation of ions. Part 5.—Gibbs free energy of hydration at 298.15 K, J. Chem. Soc. Faraday Trans., 87 (1991) 2995-2999.

[29] J. Richer, J. Lipkowski, Measurement of physical adsorption of neutral organic species at solid electrodes, J. Electrochem. Soc., 133 (1986) 121.

[30] L. Stolberg, S. Morin, J. Lipkowski, D. Irish, Adsorption of pyridine at the Au (111)-solution interface, J. Electroanal. Chem., 307 (1991) 241-262.

[31] J. Lipkowski, Building biomimetic membrane at a gold electrode surface, Phys. Chem. Chem. Phys., 12 (2010) 13874-13887.

[32] L. He, J.W. Robertson, J. Li, I. Kärcher, S.M. Schiller, W. Knoll, R. Naumann, Tethered bilayer lipid membranes based on monolayers of thiolipids mixed with a complementary dilution molecule. 1. Incorporation of channel peptides, Langmuir, 21 (2005) 11666-11672.

[33] E. Diamanti, E. Gutiérrez-Pineda, N. Politakos, P. Andreozzi, M.J. Rodriguez-Presa, W. Knoll, O. Azzaroni, C.A. Gervasi, S.E. Moya, Gramicidin ion channels in a lipid bilayer supported on polyelectrolyte multilayer films: an electrochemical impedance study, Soft matter, 13 (2017) 8922-8929.

[34] G. Valincius, T. Meškauskas, F. Ivanauskas, Electrochemical impedance spectroscopy of tethered bilayer membranes, Langmuir, 28 (2012) 977-990.

[35] G. Valincius, M. Mickevicius, Tethered phospholipid bilayer membranes: an interpretation of the electrochemical impedance response, Advances in Planar Lipid Bilayers and Liposomes, Elsevier 2015, pp. 27-61.

[36] Z. Su, J. Leitch, J. Lipkowski, Measurements of the potentials of zero free charge and zero total charge for 1-thio-±bβ-D-glucose and DPTL modified Au (111) surface in different electrolyte solutions, Z. Phys. Chem., 226 (2012) 995-1009.

[37] G. Portella, T. Polupanow, F. Zocher, D.A. Boytsov, P. Pohl, U. Diederichsen, B.L. de Groot, Design of peptide-membrane interactions to modulate single-file water transport through modified gramicidin channels, Biophys. J., 103 (2012) 1698-1705.

[38] O. Shirai, H. Yamana, T. Ohnuki, Y. Yoshida, S. Kihara, Ion transport across a bilayer lipid membrane facilitated by valinomycin, J. Electroanal. Chem., 570 (2004) 219-226.

[39] I. Burgess, M. Li, S. Horswell, G. Szymanski, J. Lipkowski, J. Majewski, S. Satija, Electric field-driven transformations of a supported model biological membrane—an electrochemical and neutron reflectivity study, Biophys. J., 86 (2004) 1763-1776.

[40] R. Lewis, R.N. McElhaney, W. Pohle, H.H. Mantsch, Components of the carbonyl stretching band in the

infrared spectra of hydrated 1, 2-diacylglycerolipid bilayers: a reevaluation, Biophys. J., 67 (1994) 2367-2375.
[41] P. Stevenson, A. Tokmakoff, Distinguishing gramicidin D conformers through two-dimensional infrared spectroscopy of vibrational excitons, J. Chem. Phys., 142 (2015) 212424.
[42] M. Zein, R. Winter, Effect of temperature, pressure and lipid acyl chain length on the structure and phase behaviour of phospholipid–gramicidin bilayers, Phys. Chem. Chem. Phys., 2 (2000) 4545-4551.
[43] A. Barth, C. Zscherp, What vibrations tell about proteins, Q. Rev. Biophys., 35 (2002) 369-430.
[44] J. Leitch, J. Kunze, J.D. Goddard, A.L. Schwan, R.J. Faragher, R. Naumann, W. Knoll, J.R. Dutcher, J. Lipkowski, In situ PM-IRRAS studies of an archaea analogue thiolipid assembled on a Au (111) electrode surface, Langmuir, 25 (2009) 10354-10363.
[45] H.L. Casal, H.H. Mantsch, Polymorphic phase behaviour of phospholipid membranes studied by infrared spectroscopy, Biochim. Biophys. Acta, 779 (1984) 381-401.
[46] T. Kim, K.I. Lee, P. Morris, R.W. Pastor, O.S. Andersen, W. Im, Influence of hydrophobic mismatch on structures and dynamics of gramicidin a and lipid bilayers, Biophys. J., 102 (2012) 1551-1560.
[47] B. Wallace, K. Ravikumar, The gramicidin pore: crystal structure of a cesium complex, Science, 241 (1988) 182-187.
[48] J.F. Nagle, S. Tristram-Nagle, Structure of lipid bilayers, Biochim. Biophys. Acta, 1469 (2000) 159-195.
[49] L. Becucci, M.R. Moncelli, R. Guidelli, Thallous ion movements through gramicidin channels incorporated in lipid monolayers supported by mercury, Biophys. J., 82 (2002) 852-864.
[50] F. Abbasi, J.J. Leitch, Z. Su, G. Szymanski, J. Lipkowski, Direct visualization of alamethicin ion pores formed in a floating phospholipid membrane supported on a gold electrode surface, Electrochim. Acta, 267 (2018) 195-205.
[51] E. Bamberg, P. Läuger, Channel formation kinetics of gramicidin A in lipid bilayer membranes, J. Membr. Biol., 11 (1973) 177-194.